PCCP

PAPER

View Article Online
View Journal

Cite this: DOI: 10.1039/d6cp00759g

Photophysical tuning *via* piperazine nitrogen torsion in a ferrocene–aminonaphthalimide derivative

Christina Eleftheria Tzeliou [a] and Demeter Tzeli *[ab]

Molecules respond to changes in their environment which may affect their photophysical properties. This computational study uses DFT and TD-DFT methods to investigate how the environmental changes tune photophysical properties in a ferrocene–aminonaphthalimide–piperazine derivative. Modeled in water and THF solvents, *via* implicit and explicit solvation, the work identifies two critical dihedral angles that influence the UV-vis absorption spectrum: piperazine N-torsion and CCNN torsion. Potential energy scans and UV-vis absorption spectra along these dihedral angles are presented. Environment affects both dihedral angles, CCNN varies with molecular substitutions, shifting the main absorption peak up to 90 nm from UV to vis area and altering its intensity, while there is also a weak peak in vis area at around 450 nm whose intensity increased with the planarity of the N atom. Overall, changes in the relative orientation of the piperazine unit to the aminonaphthalimide significantly alter the absorption spectrum. These results demonstrate that the piperazine–aminonaphthalimide geometry governs spectral behavior, illustrating how microenvironment-induced intramolecular rotations can be leveraged to tune absorption through molecular design principles.

Received 1st March 2026,
Accepted 4th May 2026

DOI: 10.1039/d6cp00759g

rsc.li/pccp

1. Introduction

The ability of molecules to process information similar to electronic systems has been proved since molecules can respond to changes in their environment, for instance presence of cations, anions or neutral species, pH, temperature, viscosity, oxidation, leading to alteration of the absorption or fluorescence spectra, *i.e.*, change of color, change of intensity or band shifts.[1–11] The development of sensors and molecular logic gates (MLGs) responsive to oxidisability and acidity that incorporate a ferrocene moiety and bioactive fluorophores have attracted research interest.[12–15] Such molecules are designed according to the principles of Photoinduced Electron Transfer (PET) systems following the 'electron donor–spacer1–fluorophore–spacer2–receptor' format, where the metallocene acts as the electron donor.

In literature, there are many research articles regarding observed shifts in absorption peaks caused by changes in molecular or lattice geometry, particularly in UV-Vis, IR, and Raman spectroscopy.[8–18] These shifts arise from alterations in electronic transitions, vibrational modes, or orbital overlaps due to steric effects, conformational changes, or structural distortions. For instance, in molecules having groups that act as donor (D) and acceptor (A) which are linked in a D–A or D–A–D format, the presence of bulky substituents in different positions on the donor groups forced the molecules to adopt geometries where the singlet charge transfer state is shifted to higher energy values, resulting in the oscillator strength and luminescence efficiency decreasing.[16] In another example, phase transitions in materials like magnesium ferrite cause cubic-to-distorted structures, splitting IR/Raman peaks due to symmetry reduction and bond length changes, while Jahn–Teller distortions or spin rearrangements further shift frequencies.[17] The solvent also affects the spectra, for instance protic solvents moderately planarize the extended π-systems, causing red-shifted absorption spectra and enhanced first hyperpolarizabilities, especially in smaller molecules *via* hydrogen bonding and geometry relaxation, while effects diminish with extended conjugation.[18]

Nitrogen atoms in organic compounds can switch between tetrahedral and planar geometries, significantly impacting UV-Vis, IR, or NMR spectra through changes in conjugation, electronic transitions, or vibrational modes.[9,10,13,15,16,19,20] Our group has reported examples of tertiary amine group linked to a fluorophore *via* spacers where the size of the spacers affects the quenching or not of the fluorescence attributed to a

[a] *Laboratory of Physical Chemistry, Department of Chemistry, National and Kapodistrian University of Athens, Panepistimiopolis Zografou, Athens 157 84, Greece. E-mail: tzeli@chem.uoa.gr; Tel: +30-210-7274307*
[b] *Theoretical and Physical Chemistry Institute, National Hellenic Research Foundation, 48 Vassileos Constantinou Ave, Athens 116 35, Greece*

PET process.[19] Furthermore, it has been shown that the geometry of the N atoms can be strongly affected by the solvent resulting in a quenching of emission spectra only for specific solvents. The complexation of cations in adjacent receptors also affects the geometry of the N atoms altering the spectra, resulting in the potential use of the compounds as sensors or MLGs.[9,10] For instance, it was found that a styryl-bodipy derivative which contains three high selective receptors for Ca^{2+}, Zn^{2+}, and Hg^{2+} is a 3-input AND MLG in aprotic solvents. The emission is accomplished by the simultaneous tetrahedral geometry of all three aniline N atoms. In acidic conditions, this was fulfilled by the existence of protons, while in acetonitrile or water solvent this is achieved *via* the existence of the three metal dications attached to the three different receptors leading to the compound emission, regardless of the complexation of the metals.[9,10]

Recently, in 2022, we studied *via* density functional theory (DFT) the photophysical properties of a 3-input AND MLG,[13] which contains a ferrocene group as an electron donor, an aminonaphthalimide as a fluorophore, and piperazine and crown ether as H^+ and Na^+ receptors, respectively; it is a 3-input MLG upon iron oxidation, protonation and Na^+ complexation. This compound had been synthesized initially by Magri *et al.*[12] and it presented an enhanced fluorescence spectrum. The calculated absorption and emission spectra were in excellent agreement with available experimental data by Magri *et al.*[12] The photophysical properties of the compounds were explained theoretically, and we demonstrated that molecular systems with N atoms, whose geometry is between planar and tetrahedral, can be excellent candidates as sensors and MLGs. It was found that small changes in the calculated geometries, specifically 7 degrees on the geometry of the N atom of piperazine, due to the explicit inclusion of the solvent, can alter the calculated UV-vis absorption and emission spectra up to 100 nm.[13] Furthermore, the transition metal that is involved in the metallocene groups affects the UV-vis spectra as well.[15] The effect of the change of the dihedral angle has been studied for specific systems. In 2024, a ferrocene-based chemosensor[20] was examined, that can generate a molecular logic circuit for the selective detection of Hg^{2+} and Cu^{2+}. The cationic sensor R responds *via* chromogenic, fluorogenic, and electrochemical channels and has multi-channel signaling capabilities. It was found that the pyridyl pyrazole rings in the optimized receptor structure exhibit an NCCN torsion angle of about 145 degrees, which is different in each case for the R–Hg^{2+} and R–Cu^{2+} molecules, indicating that the presence of metal ions results in a reduction in lone-pair repulsion. In a solvent mixture of CH_3CN and water, color changes to orange with Hg^{2+} and green with Cu^{2+}. Furthermore, fluoride sensor molecules were studied in order to identify intracellular fluoride.[21] Specifically, four *o*-bis(styryl)benzene (*o*BSB) compounds with large Stokes shifts linked to various decorating motifs that respond differentially to hydroxyl, cyanide, and fluoride ions were studied and the effect of the alteration of the dihedral angle on the value of the oscillator strength (*f*) in $S_0 \rightarrow S_1$ and the $S_0 \rightarrow S_2$ transition was studied. Ashwathi *et al.*[22] developed a sensor that employs the unique properties of anthracene for the detection of Ni^{2+}, Zn^{2+} and CN^-, among other ions. They measured specific dihedral angles of interest in the ground state, while alterations in these dihedral angles were observed upon interaction with cyanide ion. The presence of CN^- gives deep pink color to pyrrolidine-1-carbothiohydrazide (PA), while Ni^{2+} and Zn^{2+} give bright yellow color. The distinct responses of PA to CN^-, Ni^{2+} and Zn^{2+} ions allowed the sensor to develop MLGs.

In this work, we continued our two previous studies on metallocene–aminonaphthalimide–piperazine derivatives.[13,15] In ref. 15, the ferrocene–aminonaphthalimide–piperazine (**A**), see Fig. 1, the corresponding cobaltocene–aminonaphthalimide–piperazine and nickelocene–aminonaphthalimide–piperazine, the corresponding protonated, oxidized, and both protonated and oxidized species were calculated to evaluate

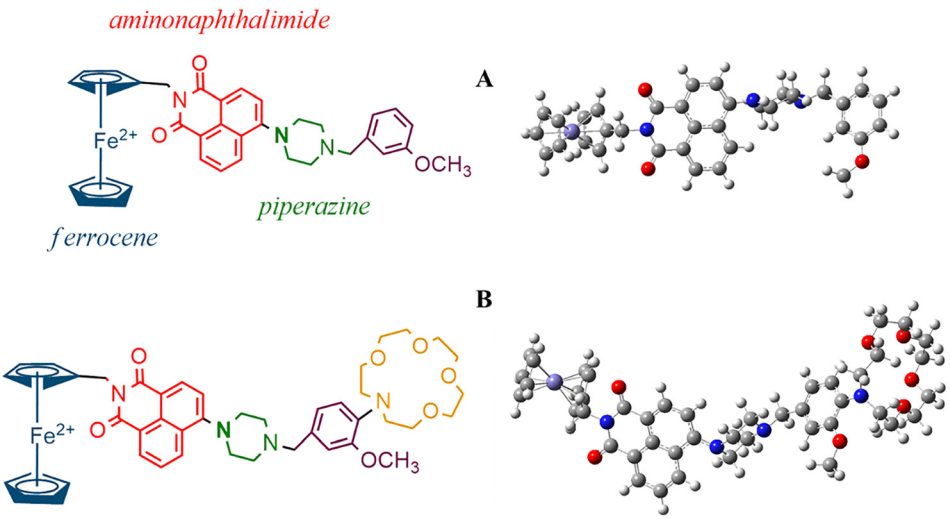

Fig. 1 Ferrocene–aminonaphthalimide–piperazine (**A**) and (ii) 3-input AND MLG (**B**).

the effect of the metal in the calculation of the absorption spectra.[15] In ref. 13, the 3-input AND MLG (**B**) was studied, which is a 3-input MLG upon iron oxidation, protonation and Na^+ complexation, along with all derivatives of **B** involved in the logic gate operation. It was found that small differences in geometry of **B**, specifically in the geometry of N atom of piperazine towards linked to aminonaphthalimide, reflect significant differences in absorption spectra, while the importance of the explicit inclusion of the solvent molecules for the accurate calculation of the UV-vis spectra for studied species was pointed out. **A** is a precursor molecule of **B**, specifically **A** has a PhOMe group, instead of PhOMe-NCrownEther group, where the PhOMe group can be symmetrically linked to piperazine group due to the absence of the N-crown ether unit. Due to the difference in these groups, these two molecules have different relative piperazine–aminonaphthalimide position and there are differences in their spectra. So, the first question that arises is: (i) does this relative position play a significant role in the calculation of the UV-vis spectra? In our previous study on **A**,[15] the THF solvent was involved only implicitly in the calculation. So, two additional questions have arisen: (ii) is the relative position of the piperazine–aminonaphthalimide affected by the explicit inclusion of one or two solvent molecules? (iii) does the type/size of the solvent affect the spectra, *i.e.*, water which is a polar protic solvent *vs* THF, which is an aprotic polar solvent having a larger size than water? Furthermore, it is important to clarify: (iv) how the changes of the observed geometry affect the absorption spectra, *i.e.*, the changes in **A** are as dramatic as in the case of the MLG where the N-crown ether was linked, adding an inherent steric restriction, and (v) are there any other parameters that may affect the spectra? Thus, the **A** molecule was investigated using DFT and TD-DFT methods in water and THF solvents, modeled both implicitly and explicitly adding one or two solvent molecules. Additionally, potential energy curves and the corresponding UV-vis spectra with respect to specific coordinates were calculated in order to obtain useful data for the manipulation of the spectra for potential applications in the design of sensors or dyes.

2. Computational methods

DFT and TD-DFT methodologies have been employed in this study to inspect the effect of the explicit solvent addition and the effect of the change of the dihedral angle of the N atom of the piperazine. All calculations were carried out using the PBE0[23,24] functional in conjunction with the 6-31G(d,p)[25] basis set in water and in tetrahydrofuran (THF) solvents employing the polarizable continuum model (PCM).[26,27] Water is a polar protic solvent with high dielectric constant, ε = 78.3553, while THF is a polar aprotic solvent, ε = 7.4257, lacking H-bond donation. Then, additional to the implicit inclusion of the solvent, one and two molecules of water or THF solvent were added next to the two N atoms of the piperazine. The structures of the molecular systems obtained are characterized as **A-W$_u$**, **A-THF$_u$**, **A-W$_d$** and **A-THF$_d$** when one molecule of the solvent has been added, where u stands for "up", *i.e.*, over the piperazine and d stands for "down", *i.e.*, below the piperazine, as plotted in Fig. 2. In the case of the addition of two solvent

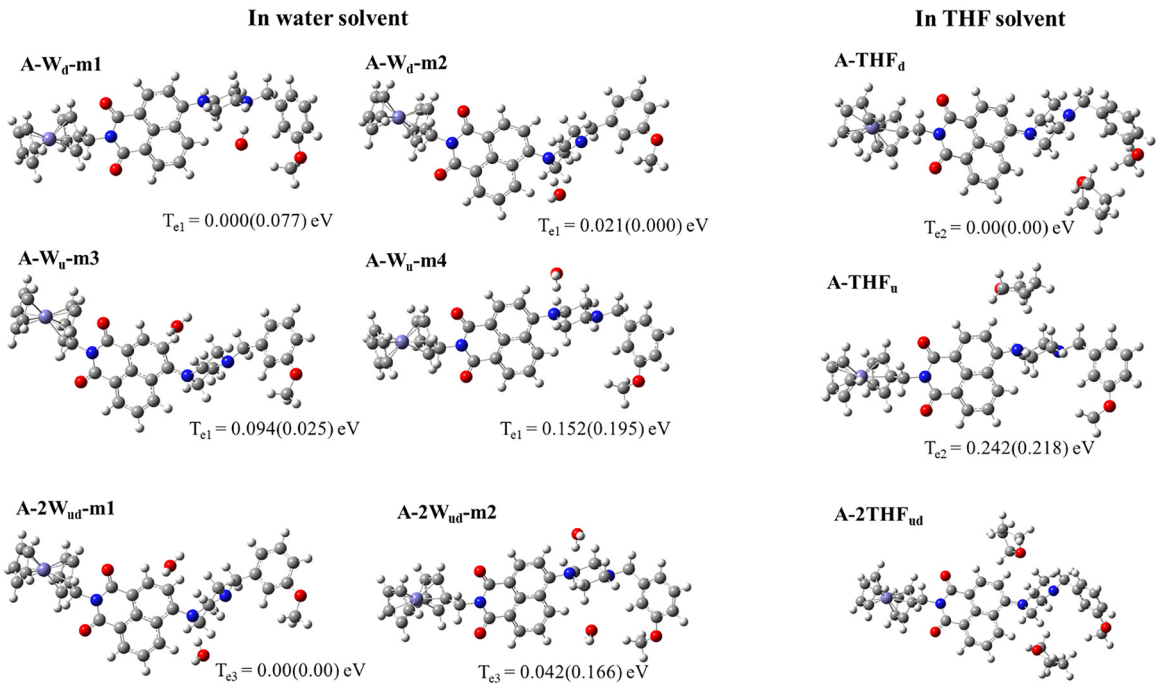

Fig. 2 Calculated minimum structures of molecule **A** with explicit addition of one and two water or THF solvent molecules and relative energies T_e at the PBE0/6-31G(d,p) and in parenthesis at the PBE0/def2-TZVP methods in water or THF solvent.

molecules, the structures are characterized as **A-2W$_{ud}$** and **A-2THF$_{ud}$**. Note that, in the case of the water solvent, two minima structures were calculated, specified as **m1** and **m2**, for instance **A-W$_u$-m1** and **A-2W$_{ud}$-m2**, as seen in Fig. 2. It should be noted that for all molecular systems, conformational analyses were carried out at first, where all species were fully energetically optimized at the PBE0/6-31G(d,p) level to locate the minimum structures presented in Fig. 2. Additionally, all calculated minimum structures were calculated at the PBE0/def2-TZVP[28] level of theory.

Regarding the methodology used, *i.e.*, PBE0/6-31G(d,p), our previous calculations on derivatives with ferrocene species, indicated that the PBE0/6-31G(d,p) level of theory[13] is a very good choice for such systems; the calculation of absorption and emission spectra is in very good agreement with available experimental data.[12] The PBE0 functional has been extensively tested for its ability to predict excited state properties, including vertical excitation energies and excited state geometries.[29,30] it has been shown that PBE0 is among the most effective functionals for the calculation of UV-vis spectra.[29] The PBE0 functional is widely used, and it is a hybrid generalized gradient approximation (GGA) functional that can provide geometry and electronic spectra in good agreement with the experiment.[31] Furthermore, additional calculations for molecule **A** using the ωB97XD,[32] and TPSSh[33] functionals in conjunction with the 6-31G(d,p) basis set, showed that all resulted in similar geometries, and B3LYP provided the same absorption spectra with PBE0, see discussion in the main text. Finally, the D3 version of Grimme's dispersion correction[34] was added to PBE0 and TPSSh functionals, *i.e.*, PBE0-D3 and TPSSh-D3, to investigate the effect of the dispersion correction in the geometry.

Potential energy curves (PEC) of the ground, singlet- and triplet- excited states with respect to the geometry of the d_2 dihedral angle (CNCC), see Fig. 3, have been plotted to study the geometry effect on the calculation of the UV-vis absorption spectra. Two PEC were plotted that correspond to different minimum structures of molecule **A** due to different position of the piperazine with respect to the aminonaphthalimide group, see Fig. 3 and discussion in the next section.

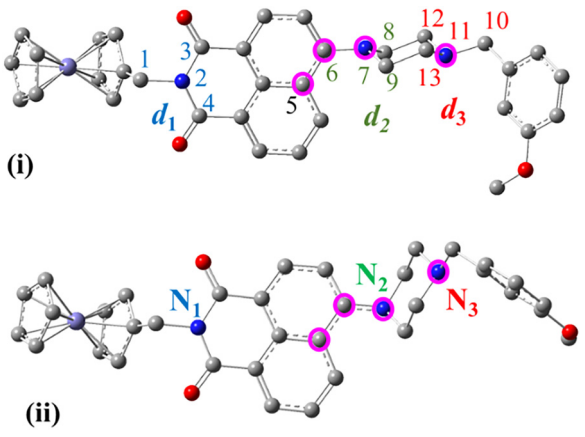

Fig. 3 CNCC dihedral angles d_1 (1,2,3,4), d_2 (6,7,8,9) and d_3 (10,11,12,13) and CCNN d_4 (5,6,7,11) dihedral angles labeled with pink rings (i) type (I) structure: aminonaphthalimide is perpendicular to the piperazine ring and (ii) type (II) structure: piperazine ring is above the aminonaphthalimide.

TD-DFT calculations were performed to obtain the absorption spectra of the structures studied in both H_2O and THF solvents. The absorption spectra of these systems were calculated including up to 50 singlet- and triplet-spin excited electronic states in all cases. The effect of explicit and implicit addition of solvent molecules in a specific position of interest was also examined. The geometry effects were studied with the computational methods mentioned above, and the respective absorption spectra were obtained. Finally, the Linear Response Correction (cLR) approach has been employed for the main absorption peaks.[35] All calculations were performed employing the Gaussian16 code.[36]

3. Results and discussion

3.1. The A, A-W, A-THF, A-2W and A-2THF molecules

Geometry. The molecule **A** in THF and water solvent has been calculated. At first, the solvent was included implicitly, then one or two solvent molecules were added so as the solvent to be included both implicitly and explicitly, see Fig. 2. The water molecules were placed next to the piperazine group because the geometry of the N atom of piperazine linked to aminonaphthalimide presents a dihedral angle ∼140 degrees and it was found that small changes in this geometry affect the absorption spectrum of derivative **B**. Four minimum structures (**A-W**) were calculated in the case of the explicit inclusion of one water molecule; their relative energy ordering is given in Fig. 2, *i.e.*, the four minimum structures are lying within 0.15 eV. Note that the three lowest-energy minima are nearly energetically degenerate at the PBE0/6-31G(d,p) method. Additional calculations at the PBE0/def2-TZVP level of theory confirm this near-degeneracy, with negligible energy differences between them. Thus, employing a larger basis set yields the same energetic picture. Two minimum structures (**A-THF**) were calculated in the case of the explicit inclusion of one THF molecule, see Fig. 2. Energetically, the solvent molecule is placed below the piperazine group for both solvent molecules, see Fig. 2. Similarly, the effect of the use of the larger basis set at the calculated relative energy is negligible, *i.e.*, the **A-THF$_u$** minimum is higher in energy than the **A-THF$_d$** by 0.242 eV at PBE0/6-31G(d,p) and 0.218 eV at PBE0/def2-TZVP. Furthermore, two water or THF solvent molecules were added above and below the piperazine group, see Fig. 2.

Furthermore, a diagnostic index for charge transfer, such as the charge transfer distance, dCT, has been calculated to justify the performance of PBE0 regarding the range-separated functionals like ωB97XD in this system. Specifically, the distance between the Fe^{2+} cation and the C_5 atom of the aminonaphthalimide, *i.e.*, the distance between the ferrocene group that act as an electron donor and aminonaphthalimide that act as an electron acceptor, was measured. It is found that the dCT values of the PBE0 and ωB97XD differ only 0.02 Å which is not a significant difference. See, Table S2 of SI.

In the case of the **A** molecule in THF solvent, the minimum structure was calculated using the PBE0, TPSSh, ωB97X-D, while the dispersion correction D3 has been added to the PBE0 and TPSSh functionals, *i.e.*, PBE0-D3 and TPSSh-D3. It is observed that all five functionals predicted similar geometries. Given that our group[13] has found that the geometry of the N atom is crucial for the calculation of the UV-vis absorption and emission spectra, the CNCC dihedral angles d_1 (1,2,3,4), d_2 (6,7,8,9) and d_3 (10,11,12,13) and the CCNC dihedral angle d_4 (5,6,7,11) of the calculated minimum structures has been computed and they are presented in Table 1 along with the $H_s\cdots N$ and $H_A\cdots O_s$ distances between each solvent molecule (s) and **A**. The minimum structures are characterized as type I or II depending on the value of the d_4 dihedral angle, see Fig. 3.

As expected, the N atom of aminonaphthalimide has a planar geometry, ∼178 degrees, while the N atom of the piperazine towards the PhOMe group has a tetrahedral geometry, ∼125 degrees. The dihedral N geometry of the piperazine towards the aminonaphthalimide ranges from 135.3 to 154.9 degrees. Furthermore, the CCNC dihedral (torsion) angle d_4 (5,6,7,11), which corresponds to the relative position of the piperazine with respect to the aminonaphthalimide, has two distinct values depending on the molecular system, *i.e.*, ∼1 degrees and ∼129 degrees that correspond to the type I and type II structures, see Fig. 3. These two dihedral angles, *i.e.*, d_2 and d_4, effect the absorption spectrum, see discussion below. In our previous study,[13] we proved the importance of the d_2 dihedral angle on the accurate calculation of the UV-vis absorption spectra, while here we further point out that the d_4 angle has two different values that affected the spectra significantly, see discussion below. Note that in our previous study on **B** and **B** derivatives,[13] the d_4 was calculated the same for all structures and thus we could not observe its importance.

Type I and type II structures have similar stability, with energy differences of up to 0.2 eV. Notably, both the PBE0/6-31G(d,p) and PBE0/def2-TZVP levels of theory yield similar relative energies. The calculated minima **A-W$_d$-m$_1$**, **A-W$_u$-m$_4$**, **A-THF$_u$**, and **A-2W$_{ud}$-m2** minimum structures correspond to type I, while **A-W$_d$-m$_2$**, **A-W$_u$-m$_3$**, **A-2W$_{ud}$-m$_1$**, **A-THF$_d$**, and **A-2THF$_{ud}$** correspond to type II, see Table 2. When one water molecule is included explicitly, type I and type II structures are energetically degenerate. However, with two explicit water molecules, the type II structure becomes the global minimum. In THF solvent, the type II structure is also the lowest-energy conformation, being ∼0.2 eV more stable than type I, see Fig. 2. Note also, that when the solvent is added implicitly only the type II structure is more stable than type I in both THF and water solvent by 0.2 eV, see Table S3 of SI.

In the **A-W**, **A-THF**, **A-2W**, and **A-2THF** molecules, hydrogen bond is formed between H atoms of **A** and the O atom of water or THF, which ranges from 2.3 to 2.5 Å. Furthermore, in four out of six **A-W** and **A-2W** molecules, hydrogen bonds are formed between the H of the water molecule and the N atom of piperazine, that range from 1.95 to 1.99 Å. In all molecular systems, the shortest observed $H_s\cdots N$ and $H_A\cdots O_s$ distances between each solvent molecule(s) and **A** are given in Table 1.

UV-vis spectra and molecular orbitals. The aim of this section is to find out how the main absorption peak of the UV-vis spectrum is affected by the d_2 and d_4 dihedral angles.

In the case of molecule **A** in THF solvent, the UV-vis absorption spectrum was calculated using the PBE0, TPSSh, ωB97X-D, PBE0-D3 and TPSSh-D3 functionals. It is observed that the PBE0 and PBE0-D3, in the geometry calculated with the inclusion of the dispersion forces, predict a main peak at 334 nm, the ωB97X-D functional predicts a peak at 309 nm,

Table 1 Selected geometries, CNCC dihedral angles d_1 (1,2,3,4), d_2 (6,7,8,9) and d_3 (10,11,12,13) in degrees, CCNC dihedral angle d_4 (5,6,7,11) in degrees, and the $H_s\cdots N$ and $H_A\cdots O_s$ distances[a] in Å (see Fig. 3) of the **A**, **A-W**, **A-2W**, **A-THF** and **A-2THF** molecular systems in water or THF solvent at the PBE0, TPSSh, ωB97X-D, PBE0-D3, TPSSh-D3/6-31G(d,p) level of theory

Molecule	Method	Solvent	d_1	d_2	d_3	d_4	Type[a]	$H_s\cdots N$[b]	$H_A\cdots O_s$[b]
A	PBE0[c]	THF	178.2	141.8	124.9	0.06	I		
	PBE0-D3	THF	175.9	140.9	125.7	1.54	I		
	TPSSh[c]	THF	178.9	140.1	124.3	1.13	I		
	TPSSh-D3	THF	173.8	138.9	125.0	1.73	I		
	ωB97XD[c]	THF	176.1	141.4	125.4	1.58	I		
	PBE0	THF	177.7	150.2	124.9	129.6	II		
	PBE0	THF	178.9	149.2	124.5	90.5	ts		
	PBE0	Water	178.6	141.6	124.8	0.23	I		
	PBE0	Water	178.0	151.3	124.9	129.1	II		
	PBE0	Water	178.5	147.6	124.5	85.9	ts		
A-W$_d$-m$_1$	PBE0	Water	178.7	138.6	122.9	0.54	I	3.317	2.452
A-W$_d$-m$_2$	PBE0	Water	179.3	141.2	124.7	129.5	II	1.975	2.458
A-W$_u$-m$_3$	PBE0	Water	179.6	151.9	124.7	128.7	II	3.493	2.558
A-W$_u$-m$_4$	PBE0	Water	178.5	135.5	124.6	1.62	I	1.953	2.373
A-2W$_{ud}$-m$_1$	PBE0	Water	179.3	141.9	124.3	128.6	II	1.989 (d), 3.745 (u)	2.461 (d), 2.544 (u)
A-2W$_{ud}$-m$_2$	PBE0	Water	178.7	135.3	124.4	3.39	I	4.870 (d), 1.956 (u)	2.357 (d), 2.328 (u)
A-THF$_u$	PBE0	THF	178.3	140.8	124.9	0.33	I	3.290	2.282
A-THF$_d$	PBE0	THF	177.8	150.9	125.6	129.6	II	5.138	2.444
A-2THF$_{ud}$	PBE0	THF	177.7	154.9	125.1	127.5	II	4.744 (d), 3.637 (u)	2.374 (d), 2.301 (u)

[a] Type I or II, see Fig. 3; ts: transition state between type I and type II. [b] The shortest $H_s\cdots N$ and $H_A\cdots O_s$ distances between **A** and **W** or **THF** solvent molecule, where H_s: hydrogen atom of the solvent, O_s: hydrogen atom of the solvent. [c] Ref. 15.

Table 2 Main absorption peaks, λ (nm), energy differences ΔE (eV), f-values and the corresponding main excitations of the absorption spectrum of the **A**, **A-W**, **A-2W**, **A-THF** and **A-2THF** molecular systems in water or THF solvent at the PBE0, TPSSh, ωB97X-D, PBE0-D3, TPSSh-D3/6-31G(d,p) level of theory. LR corrected ΔE values (eV) are given in parentheses

Molecule	Method	Solvent	d_4	λ	ΔE	f	Main excitation
A	PBE0[a]	THF	0.39	333.5	3.72	0.4260	0.989 |H-6 → L⟩
	PBE0-D3	THF	1.54	333.5	3.72	0.4250	0.986 |H-6 → L⟩
	ωB97XD[a]	THF	1.58	308.9	4.01	0.5029	0.916 |H-5 → L⟩
	TPSSh[a]	THF	1.13	353.5	3.51	0.2344	0.768 |H-6 → L⟩
	TPSSh-D3	THF	1.73	353.9	3.50	0.2740	0.833 |H-6 → L⟩
	PBE0	Water	0.39	333.5	3.72	0.4216	0.989 |H-6 → L⟩
B[b]	PBE0	Water	129.24	420.0	2.95 (2.93[c])	0.3932	
B-W[c]	PBE0	Water	129.09	401.4	3.09 (3.03[c])	0.3396	
	Expt[d]	Water		400			
A-W$_d$-m$_1$	PBE0	Water	0.54	334.2	3.71 (3.71)	0.4208	0.981 |H-5 → L⟩
A-W$_d$-m$_2$	PBE0	Water	129.47	399.9	3.10 (3.05)	0.3391	0.990 |H-2 → L⟩
A-W$_u$-m$_3$	PBE0	Water	128.70	417.2	2.97 (2.95)	0.3661	0.879 |H-2→ L⟩
A-W$_u$-m$_4$	PBE0	Water	1.62	332.8	3.73 (3.76)	0.4218	0.979 |H-5 → L⟩
A-2W$_{ud}$-m$_1$	PBE0	Water	128.59	401.8	3.09 (3.03)	0.3231	0.991 |H-2 → L⟩
A-2W$_{ud}$-m$_2$	PBE0	Water	3.39	333.7	3.72 (3.72)	0.2547	0.733 |H-5 → L⟩
A-THF$_d$	PBE0	THF	129.59	418.9	2.96 (2.95)	0.3914	0.812 |H-2→ L⟩
A-THF$_u$	PBE0	THF	0.33	334.2	3.71 (3.71)	0.4152	0.981 |H-6 → L⟩
A-2THF$_{ud}$	PBE0	THF	127.47	421.5	2.94 (2.94)	0.4067	0.988 |H → L⟩

[a] Ref. 15. [b] Ref. 13, LR corrected value: 422.8 nm. [c] Ref. 13, one water molecule has been added explicitly, and it interacts with molecule B LR corrected value: 408.7 nm. [d] Ref. 12.

while TPSSh and TPSSh-D3 predict a main peak at 354 nm. The ωB97X-D functional predicts the highest oscillator strength, while the TPSSh predicts the lowest one. In water solvent, the main peak was calculated at 334 nm *via* the PBE0 functional. Thus, depending on the functional, the absorption peak is shifted up to 45 nm. Our previous study[13] on a derivative of **A**, *i.e.*, on the MLG **B** which contains a PhOMe-NCrownEther unit while **A** has a PhOMe group, has shown that the PBE0/6-31G(d,p) method is very good choice for the accurate calculation of the UV-vis absorption spectra since it predicts accurately the experimentally measured main absorption peak. Specifically, the main absorption peak in water solvent was calculated at 420 nm for **B** and at 401 nm for **B-W**, where a water molecule has also been added explicitly. The experimental absorption peak was measured at 400 nm, in excellent agreement with our calculated values. Thus, the PBE0/6-31G(d,p) method is a very good choice for this type of molecular systems and so this method was used for all calculated molecular systems of the present study.

The absorption spectrum of the calculated minimum structures of the **A**, **A-W**, **A-2W**, **A-THF** and **A-2THF** molecular systems in water or THF solvent at the PBE0/6-31G(d,p) level of theory has been plotted in Fig. 4. Selected main peaks are given in Table 2. The cLR approach was employed, and its effect was found to be negligible. The absorption peaks shift by at most 8 nm (0.05 eV), indicating a limited impact of the cLR correction, see Table 2 and Table S6 of SI. This behavior suggests that the excited states involved do not exhibit purely long-range charge-transfer character but rather a mixed local/CT nature, which reduces their sensitivity to state-specific solvent polarization. However, the main reason for the limited impact of the cLR correction is that the solvent polarization is already adequately represented by the hybrid solvation approach with one or two explicit molecules. Previous theoretical studies from our group on the UV-vis spectra of caffeine in ambient liquid water have shown that including solvent effects both explicitly and implicitly yields accurate agreement with experimentally measured spectra.[37]

It is found that the calculated absorption spectra are separated into three groups, the first one has a main peak at ~420 nm, the second one at 400 nm and the third one at 334 nm. As mentioned above, the CCNN dihedral (torsion) angle d_4 (5,6,7,11), which corresponds to the relative position of the piperazine with respect to the aminonaphthalimide, has two distinct values depending on the molecular system, *i.e.*, ~1 degrees and ~129 degrees. The first value corresponds to a perpendicular position of piperazine with respect to aminonaphthalimide group. As shown in Table 2, when d_4 dihedral

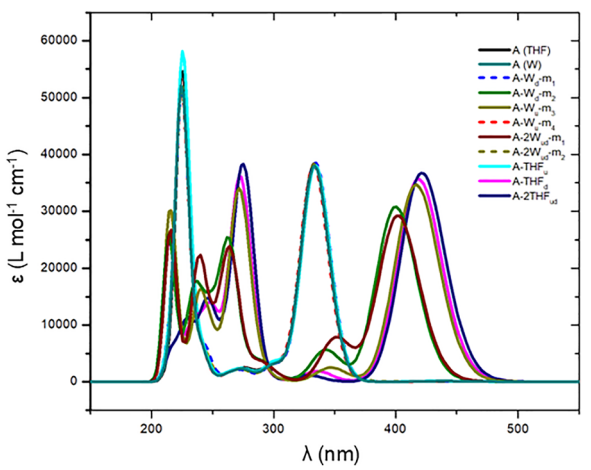

Fig. 4 Absorption spectrum of the calculated minimum structures of the **A**, **A-W**, **A-2W**, **A-THF** and **A-2THF** molecular systems in water or THF solvent at the PBE0/6-31G(d,p) level of theory.

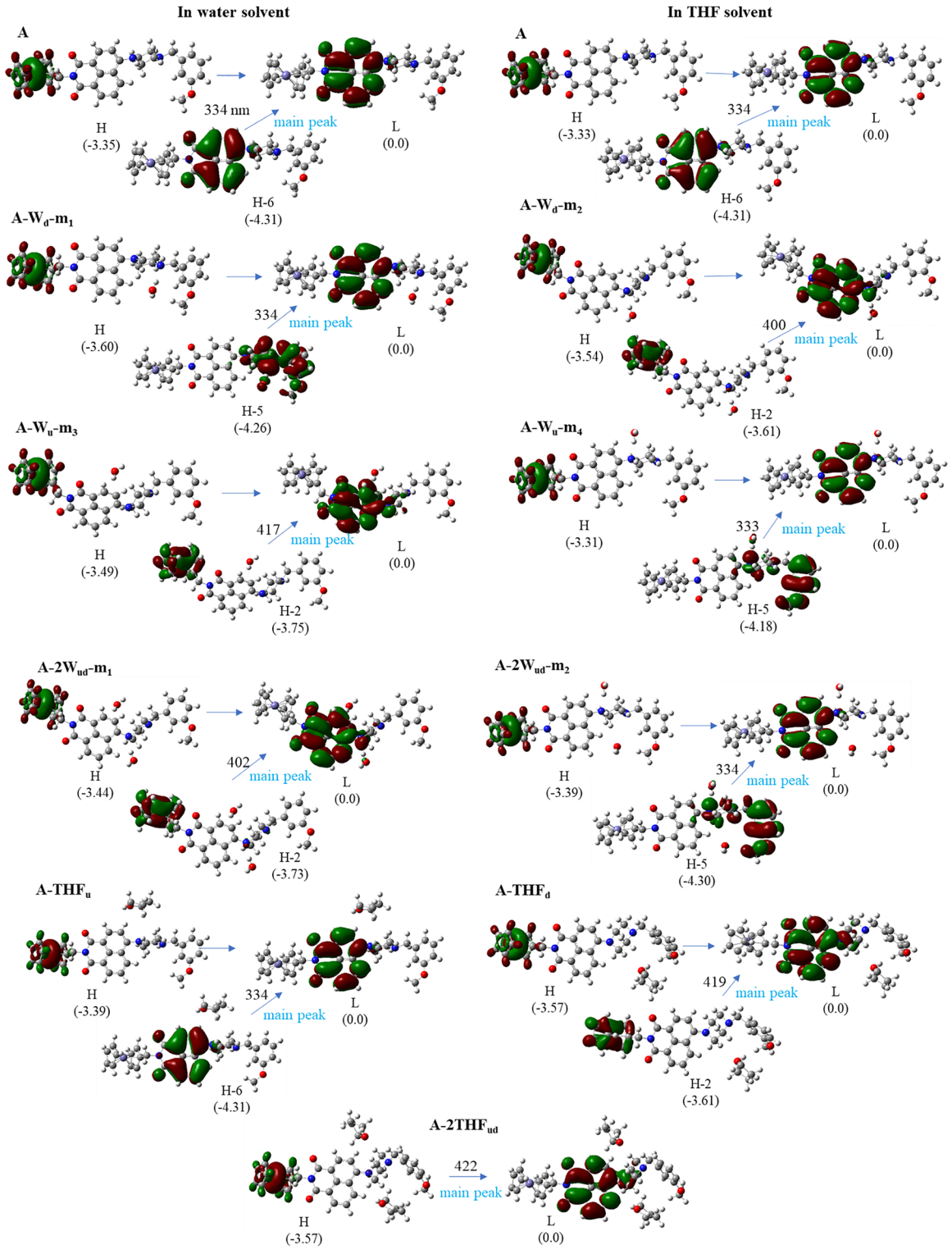

Fig. 5 Electron density plots of the molecular orbitals involved in the H → L excitation and to the major UV-vis absorption peak of the calculated minimum structures at the PBE0/6-31G(d,p) in the THF and water solvent. Their relative energies of MO are given in eV.

angle is about 1 degree, the d_2 dihedral angle ranges from 135 to 141 degrees and the first main absorption peak is about 334 nm, while when d_4 dihedral angle is about 129 degrees, the d_2 dihedral angle ranges from 141 to 155 degrees and the first main absorption peak ranges from λ = 400 nm to λ = 422 nm and the largest λ values correspond to largest d_2 angles. Overall, the environment, *i.e.*, addition of solvent molecules, affects both d_2 and d_4 dihedral angles. On the contrary, the addition of an N-crown ether on the PhOMe unit results in molecular structures having d_4 values of ~129 degrees only, meaning that

the substitution with a large unit affects only d_4 due to the steric restrictions. Thus, the values of both d_2 and d_4 can be tuned.

For all calculated molecular structures, the $|H \rightarrow L\rangle$ excitation corresponds to an electron transfer excitation from the ferrocene group to aminonaphthalimide, see Fig. 5. For **A** in both water and THF and for **A-THF$_u$**, the first main UV-vis absorption peak retains the electron density in aminonaphthalimide with a λ value of 334 nm, see Fig. 4. On the contrary, the first main UV-vis absorption peak for the **A-W$_d$-m$_1$**, **A-W$_u$-m$_4$**, and **A-2W$_{ud}$-m$_2$** structures corresponds to an electron transfer from piperazine-PhOMe to the aminonaphthalimide, Fig. 4, and λ values of 334 nm. For the **A-W$_d$-m$_2$**, **A-W$_u$-m$_3$**, **A-2W$_{ud}$-m$_1$**, **A-THF$_d$**, and **A-2THF$_{ud}$** structures, it corresponds to an electron transfer from the ferrocene group to aminonaphthalimide with λ values of 400–422 nm, Fig. 4. Furthermore, it should be noted that in all molecular systems there is a main peak in UV area at about 225 nm which results in a $|H\text{-}6 \rightarrow L + 1\rangle$ excitation. As a final comment, the main excitations of the selected peaks for the global minima of **A-W**, **A-2W**, **A-THF**, and **A-2THF** exhibit coefficients of about 0.98 (see Table 2), indicating that frontier molecular orbitals accurately describe the electron density distribution. NTO analysis for representative systems **-2W$_{ud}$-m$_1$** and **A-2W$_{ud}$-m$_2$** see Fig. S2 of SI, confirms identical spatial electron density and charge-transfer characteristics.

To sum up, there is no significant change in the absorption spectrum of **A** resulting from the use of water or THF solvent. The explicit inclusion of one solvent molecule can lead to two minimum structures with different d_4 dihedral angles and thus difference in the position of the first main peak at about 334 or 400 or 420 nm depending also on the d_2 dihedral angle. The best structures that can predict the experimental absorption spectrum arise upon addition of two solvent molecules. The corresponding lowest in energy structures present the main peak in vis area at 402 nm in water and 422 nm in THF.

3.2. Potential energy curves and excited states

Recently, it was found that the d_2 value affects the absorption spectrum of molecule **B** and its protonated, oxidized, and complex structure with Na^+ cation.[13] Here, we study its precursor molecule **A**, and we found that the d_2 value also affects the absorption spectrum but additionally, we found that the dihedral angle d_4 presents two distinct values that also affect the absorption spectrum. The torsion d_4 value is related with the relative position of the piperazine with respect to the aminonaphthalimide group.

In order to investigate the geometry effect on the calculation of the UV-vis absorption spectra, the PEC of the ground, singlet- and triplet- excited states with respect to the geometry of the d_2 dihedral angle (Fig. 3) have been plotted. Two PEC were plotted that correspond to different minimum structures of molecule **A** due to different favored positions of the piperazine, *i.e.*, type (I) structure: the aminonaphthalimide is perpendicular to the piperazine ring and type (II) structure: piperazine ring is above the aminonaphthalimide with a d_4 of 129 degrees, see Fig. 6.

The potential energy curves of 50 singlets and 50 triplets for the structures I and II are given in Fig. 6. The ground S_0 state is well separated from the excited states. The T_1 state is lying about 1.65 eV above the S_0 state corresponding to an λ value of 753 nm for type I and 1.69 eV above the S_0 state corresponding to an λ value of 736 nm for type II. The following six triplet states (T_2 to T_7) are also lower in energy than the S_1 excited state. The excited states are closely lying and avoided crossings are observed between (S_1 and S_2) and (T_7 and T_8) for type I, see Fig. 6a. Finally, it should be noted that the PECs of the electronic excited states form bands of very close lying state, see Fig. 6. Some differences are observed between the PECs of the two structures, *i.e.*, in type II the PECs are higher in energy by 0.5 eV on average, but overall, the general shape is the same.

The potential energy curves in Fig. 6 directly link molecular conformation to fluorescence behavior. For the type I structure ($d_4 \approx 1$ degrees), the S_1 state remains well-separated from both the ground state and the triplet manifold (T_1 to T_6 states) along the d_2 coordinate, with moderate ΔE variations. However, avoided crossings occur between S_1 and S_2 and between T_7 and T_8, located at global minima with a d_2 value of 151 degrees. Note that the S_0 minimum has d_2 = 141.8 degrees. The S_1 relaxation pathway may enable intersystem crossing ($S_1 \rightarrow T_1$) and then phosphorescence. In contrast, the type II structure

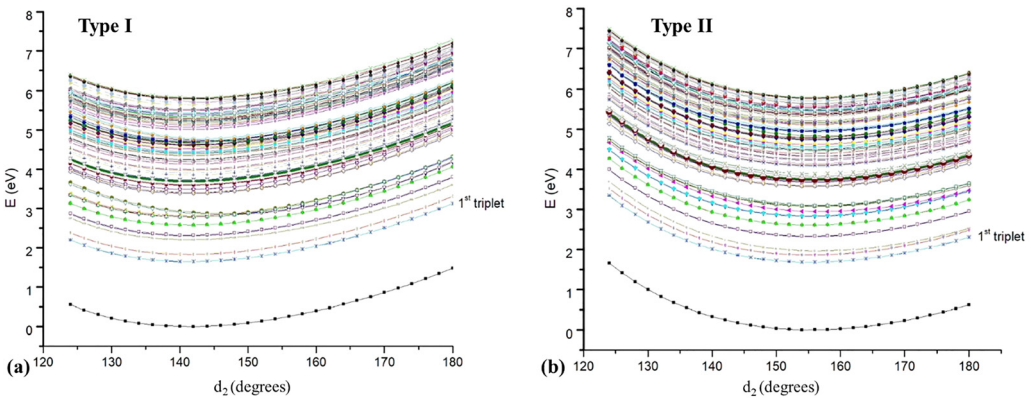

Fig. 6 Potential energy curves of the 50 singlet- and 50 triplet-spin electronic states of **A** with respect to the dihedral angle d_2 of (a) type I structure and (b) type II structure at the PBE0/6-31G(d,p) level of theory in THF solvent.

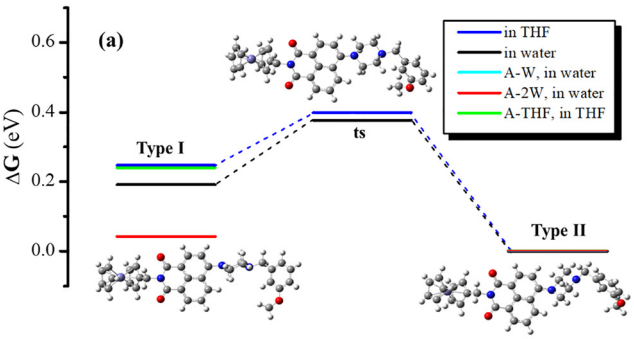

(b)

	Barrier (eV)	ΔG‡ (kJ/mol)	Rate Constant (s^{-1})	Lifetime (μs)
I → II in THF	0.152	14.7	1.5×10^{8}	0.007
II → I in THF	0.399	38.5	3.2×10^{3}	310
I → II in water	0.186	18.0	2.0×10^{7}	0.05
II → I in water	0.377	36.4	1.3×10^{4}	77

Fig. 7 (a) Relative Gibbs free energies for the I ↔ II interconversion of **A**, **A-W**, **A-W$_2$**, and **A-THF** with respect to type II (type II is lying at 0 level) and (b) rate constants of **A** interconversion at the PBE0/6-31G(d,p) level of theory in water and THF solvent including the solvent implicitly.

($d_4 \approx 129$ degrees) exhibits near-degenerate S_1 and S_2 states, both well-separated from nearby triplets, favoring fluorescence. Ferrocene serves as the primary PET donor, aminonaphthalimide acts as an acceptor with piperazine orientation (d_4) controlling also the coupling. Thus, type II's perpendicular piperazine ($d_4 \approx 129$ degrees) may suppress PET, enhancing fluorescence. For this reason, molecule B presenting only the stable type II conformer, *i.e.*, type I is unstable, shows enhanced fluorescence.[13]

Furthermore, the dynamic of the interconversion of type I to type II has been examined when the solvent is added implicitly. Type II structure is more stable than type I in both THF and water solvent by about 0.2 eV (electronic energy). Similarly, the relative Gibbs free energy ΔG is 0.191 (0.247) eV in water (THF) solvent, while the transition state connected the two minima is 0.377 (0.399) eV above the global minimum of II type, see Fig. 7. Using Eyring transition state theory, $k = \frac{k_B T}{h} e^{-\Delta G^{\ddagger}/RT}$, where $\Delta G^{\ddagger}$ is 0.377 (0.399) eV, for the interconversion II → I, $k = 1.3 \times 10^4\ s^{-1}$ ($32 \times 10^3\ s^{-1}$) at room temperature (298 K), while for the interconversion I → II, where $\Delta G^{\ddagger} = 0.186$ (0.152) eV, $k = 2.0 \times 10^7\ s^{-1}$ ($1.5 \times 10^8\ s^{-1}$), see Fig. 7. So, type II is kinetically stable. However, explicit solvation can yield near-degenerate conformers (*e.g.*, **A-W$_d$-m$_1$** *vs.* **A-W$_d$-m$_2$**), potentially observable spectroscopically. Other specialized conditions, such as cryogenic temperatures, glassy matrices, or host–guest nanoconfinement, can further resolve both type I and type II conformers by kinetic trapping.

The absorption spectrum of structures I with respect to the d_2 dihedral angle is plotted in Fig. 8a. There are three main peaks of interest. The first one is in the area of 200–250 nm, the second in 300–350 nm and the last one in 430–500 nm. It found that as the d_2 changes from 124 degrees (tetrahedral geometry) to 180 degrees (planar geometry) the intensity of the first peak is increased and it is red shifted up to 459 nm (180 degrees). This peak corresponds to an electron transfer peak from the ferrocene to the aminonaphthalimide group, see Fig. 9. The main peak at 334 nm is blue shifted slightly up to 327 nm, while its intensity is decreased with the increase of the d_2 value, however it remains to be the main peak in the area 250 nm to 600 nm, see Table 3. This main peak does not have any charge transfer character, and the electron density is located at the aminonaphthalimide group, see Fig. 9. On the contrary, a third peak at about 275 nm is observed, where its intensity increases with the increase of the d_2 value. Finally, the peak at 225 nm remains sharp and intense for all d_2 values, without any significant changes.

The absorption spectrum of structures II with respect to the d_2 dihedral angle is plotted in Fig. 8b. There are four main

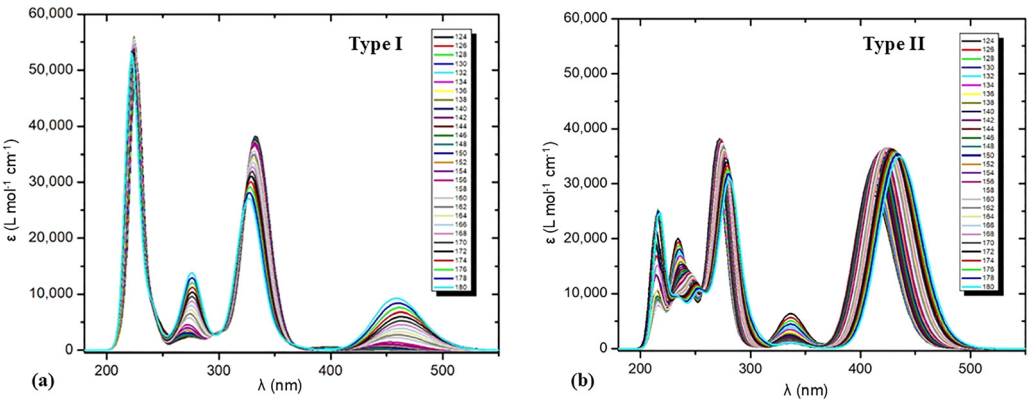

Fig. 8 Absorption spectrum of the calculated structures for different d_2 dihedral angles of (a) type I structure and (b) type II structure at the PBE0/6-31G (d,p) level of theory in THF solvent.

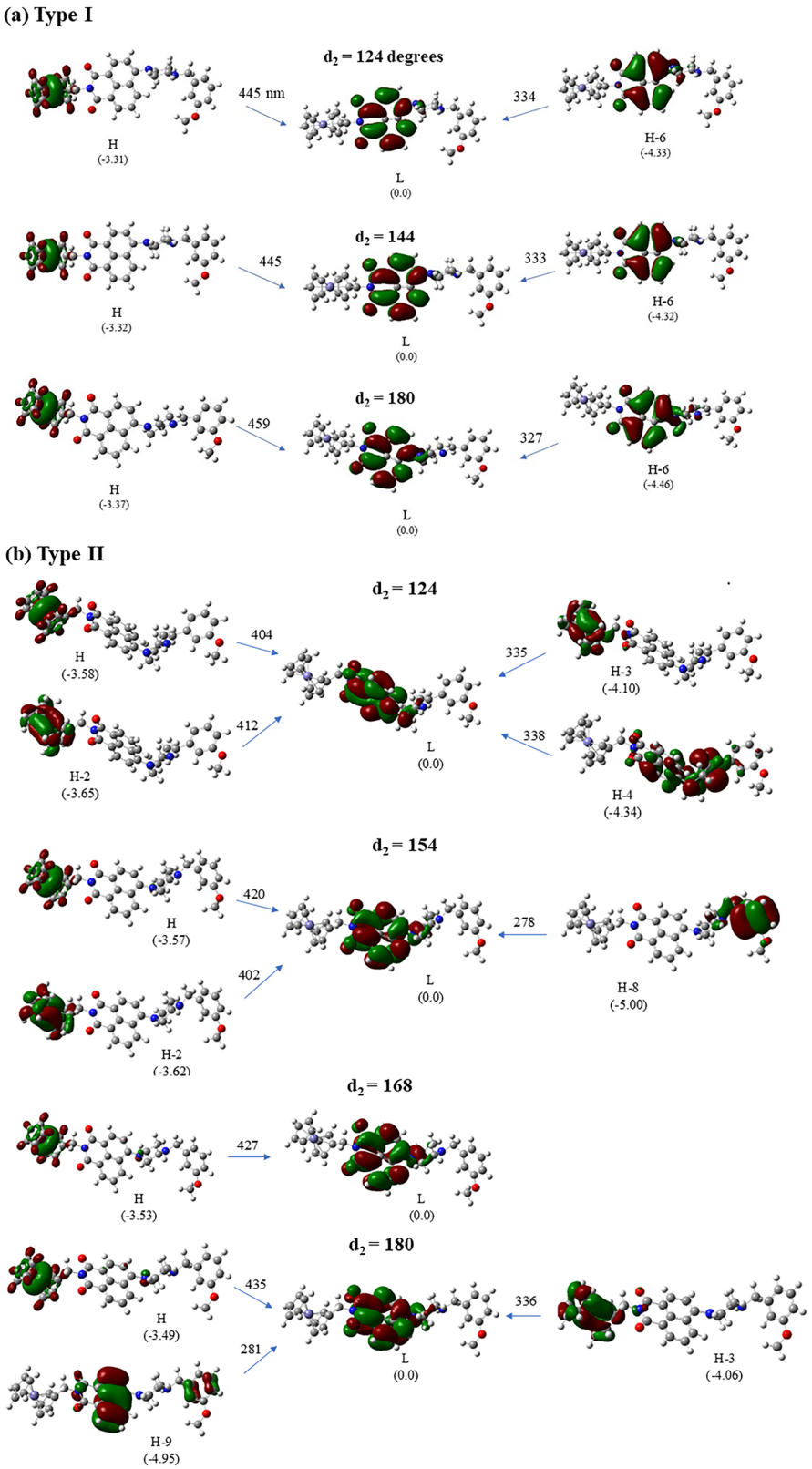

Fig. 9 Frontiers molecular orbitals involved in main UV-vis absorption peaks of (a) type I and (b) II for specific d_2 dihedral angles at the PBE0/6-31G(d,p) level of theory in THF solvent. Relative energies of orbitals in eV are included with respect to L orbital.

Table 3 Absorption peaks, λ (nm), energy differences ΔE (eV), f-values and the corresponding main excitations of the type I and II structures at the PBE0/6-31G(d,p) level of theory

Type	d_2	λ	ΔE	f	Main excitation
I	124	445.4	2.78	0.0009	0.840 |H → L⟩
		333.5	3.72	0.4183	0.967 |H-6→ L⟩
	144	445.0	2.79	0.0009	0.834 |H → L⟩
		332.6	3.73	0.4242	0.990 |H-6→ L⟩
	180	458.9	2.70	0.1020	0.829 |H-2 → L⟩
		326.7	3.80	0.3007	0.971 |H-6→ L⟩
II	124	412.0	3.01	0.2969	0.868 |H → L⟩
		337.6	3.67	0.0506	0.818 |H-4 → L⟩
	154	419.8	2.95	0.3982	0.939 |H → L⟩
		336.3	3.69	0.0117	0.930 |H-4 → L⟩
	168	426.9	2.91	0.4017	0.966 |H → L⟩
		337.5	3.67	0.0087	0.918 |H-4 → L⟩
	180	435.2	2.85	0.2935	0.851 |H → L⟩
		339.4	3.65	0.0068	0.833 |H-4 → L⟩

peaks of interest, *i.e.*, the first one is in the area of 200–240 nm, the second in 260–280 nm, the third in 300–350 nm and the last one in 400–450 nm. It found that as the d_2 changes from 124 degrees (tetrahedral geometry) to 180 degrees (planar geometry), the main peak at 412 nm is red shifted at 435 nm. Similar red shifts are observed for peaks at ∼270 nm and ∼230 nm, while their intensity is decreased, see Fig. 8. On the contrary, the observed peak at the 340 nm does not shift with the increase of the d_2 dihedral angle, but its intensity is decreased significantly. The peak at ∼420 nm corresponds to a charge transfer from ferrocene to aminonaphthalimide, see Fig. 9. The peak at ∼340 nm also corresponds to a charge transfer from ferrocene to aminonaphthalimide, while there are closely lying peaks that retain the electron density at aminonaphthalimide. Finally, the peaks at ∼270 nm present charge transfer excitation from PhOMe to aminonaphthalimide.

Overall, the differences in d_2 and d_4 dihedral angles result in shifts of the UV-vis absorption peaks and changes in their intensity. So, when the piperazine is perpendicular to the plane of the aminonaphthalimide (type I), **A** presents a main peak in vis area at around 450 nm, however when piperazine is not perpendicular and the CCNN is about 129 degrees (type II), the corresponding main peak is around 420 nm and is enhanced significantly. In solution at room temperature when the solvent is added implicitly only, type II is kinetically stable. However, explicit solvation yields energetically degenerate type I and II conformers in water, enabling kinetic trapping of both, whereas type II remains more stable than type I in THF. Furthermore, the substitution of the PhOMe group with a group as the N-crown ether in molecule **B**,[13] results only in one conformer and the d_4 dihedral angle presents a tetrahedral geometry and thus the intensity of the vis absorption peak will be greatly enhanced. To sum up, these findings demonstrate piperazine-aminonaphthalimide geometry as a conformational switch, with microenvironments driving spectral tuning *via* intramolecular rotations—offering design principles for sensors and dyes.

4. Summary and conclusions

In this work, we studied molecule **A**, a ferrocene–aminonaphthalimide–piperazine derivative *via* DFT and TD-DFT methodology in both water and THF solvent. The solvent was employed either implicitly or both implicitly and explicitly *via* the inclusion of one or two solvent molecules in addition to the PCM model.

Two dihedral angles affect significantly the absorption spectrum, (i) the N torsion angle of the piperazine toward to aminonaphthalimide (d_2) that ranges from 135.3 to 154.9 degrees and (b) the CCNN dihedral (torsion) angle (d_4) which corresponds to the relative position of the piperazine with respect to the aminonaphthalimide. The last one was found to have two distinct values depending on the molecular system, *i.e.*, ∼1 degrees and ∼129 degrees. In our previous study,[13] we proved only the importance of the d_2 dihedral angle on the accurate calculation of the UV-vis absorption spectra on derivatives of the present molecule in water solvent, where the corresponding d_4 angle remained the same in all calculated molecular systems. Here, we point out that (a) environment affects both the d_2 and d_4 dihedral angle resulting in shifts of the UV-vis spectra and (b) the d_4 angle has two different values depending on the derivative of the PhOMe group, which affected significantly the spectra shifting the main peak in the vis area and increasing significantly its intensity. Thus, the d_4 torsion angle is the key angle on the design of molecules with specific properties.

Overall, the absorption spectrum of **A** is not significantly affected by the use of either water or THF as the solvent. However, the explicit inclusion of a single solvent molecule yields two distinct minimum-energy structures with different d_4 dihedral angles, resulting in observing the first major absorption peak either at 334 nm or at 400 nm and 420 nm. The shift of 20 nm depends on the value of d_2 dihedral angle. The structures that best reproduce the experimental absorption spectrum are obtained when two solvent molecules are included. In these lowest-energy configurations, the main absorption band appears in the visible region at 402 nm in water and 422 nm in THF.

Potential energy curves and the absorption spectra have been plotted with respect to the change of the d_2 dihedral angle for two main values of the d_4 dihedral angle. Overall, the differences in d_2 and d_4 dihedral angles result in shifts of the UV-vis absorption peaks and changes in their intensity. So, when the piperazine is perpendicular to the plane of the aminonaphthalimide (type I), **A** presents a main peak in vis area at around 450 nm, however when piperazine is not perpendicular and the CCNN is about 129 degrees (type II), the corresponding main peak is around 420 nm and is enhanced significantly. At room temperature, type II exhibits kinetic stability under implicit solvation. However, explicit solvation can yield near-degenerate type I and II conformers in specific solvents. Specialized conditions, such low temperatures, glassy matrices, or host–guest nanoconfinement, can thus kinetically isolate and spectroscopically resolve both conformers. Furthermore, the substitution of the PhOMe group

with a group as the N-crown ether in molecule **B**,[13] results only in a stable type II confirmer only which present an enhanced intensity of the vis absorption peak.

Thus, changes in the relative position of the piperazine unit with respect to the aminonaphthalimide result in significant changes in the absorption spectrum. Consequently, manipulation of the environment around the molecule, either by solvent choice or constraint spaces such as cavities, can lead to changes in the UV-vis spectra. This study demonstrates how microenvironments tune absorption spectra *via* intramolecular rotations for sensing applications guiding multiconformer modeling in computational chemistry.

Conflicts of interest

The authors have no conflicts to disclose.

Data availability

The data that support the findings of this study are available within the article and its supporting information (SI). Supplementary information: geometry, absorption spectrum data. See DOI: https://doi.org/10.1039/d6cp00759g.

Acknowledgements

CET acknowledges the Hellenic Foundation for Research and Innovation for the financial support of this project under the 5th Call for HFRI PhD fellowships (fellowship number: 21006).

References

1 A. P. de Silva, H. Q. N. Gunaratne and C. P. McCoy, A molecular photoionic AND gate based on fluorescent signalling, *Nature*, 1993, **364**, 42–44.
2 T. Konry and D. R. Walt, Intelligent Medical Diagnostics via Molecular Logic, *J. Am. Chem. Soc.*, 2009, **131**, 13232–13333.
3 D. C. Magri and A. P. de Silva, From PASS 1 to YES to AND logic: building parallel processing into molecular logic gates by sequential addition of receptors, *New J. Chem.*, 2010, **34**, 476–481.
4 J. Andréasson and U. Pischel, Smart molecules at work---mimicking advanced logic operations, *Chem. Soc. Rev.*, 2010, **39**, 174–188.
5 J. Ling, B. Daly, V. A. D. Silverson and A. P. de Silva, Taking baby steps in molecular logic-based computation, *Chem. Commun.*, 2015, **51**, 8403–8409.
6 D. Tzeli, I. D. Petsalakis and G. Theodorakopoulos, Molecular logic gates based on benzo-18-crown-6 ether of styrylquinoline: a theoretical study, *Phys. Chem. Chem. Phys.*, 2016, **18**, 32132–32145.
7 S. Erbas-Cakmak, S. Kolemen, A. C. Sedgwick, T. Gunnlaugsson, T. D. James, J. Yoon and E. U. Akkaya, Molecular logic gates: the past, present and future, *Chem. Soc. Rev.*, 2018, **47**, 2228–2248.
8 J. Andréasson and U. Pischel, Molecules for security measures: from keypad locks to advanced communication protocols, *Chem. Soc. Rev.*, 2018, **47**, 2266–2279.
9 D. Tzeli, I. D. Petsalakis and G. Theodorakopoulos, Theoretical study of the photophysical processes of a styryl-bodipy derivative eliciting an AND molecular logic gate response, *Int. J. Quantum Chem.*, 2019, **119**, e25958.
10 D. Tzeli, I. D. Petsalakis and G. Theodorakopoulos, The solvent effect on a styryl-bodipy derivative functioning as an AND molecular logic gate, *Int. J. Quantum Chem.*, 2020, **120**, e26181.
11 D. C. Magri, Logical sensing with fluorescent molecular logic gates based on photoinduced electron transfer, *Coord. Chem. Rev.*, 2021, **426**, 213598.
12 G. J. Scerri, J. C. Spiteri, C. J. Mallia and D. C. Magri, A lab-on-a-molecule with an enhanced fluorescent readout on detection of three chemical species, *Chem. Commun.*, 2019, **55**, 4961–4964.
13 C. E. Tzeliou and D. Tzeli, 3-input AND molecular logic gate with enhanced fluorescence output: The key atom for the accurate prediction of the spectra, *J. Chem. Inf. Model.*, 2022, **62**, 6436–6448.
14 J. Grech, J. C. Spiteri, G. J. Scerri and D. C. Magri, Molecular logic with ferrocene-rylene conjugates: A comparison of naphthalenediimide, naphthalimide and perylenediimide Pourbaix sensor designs, *Inorg. Chim. Acta*, 2023, **544**, 121176.
15 C. E. Tzeliou and D. Tzeli, Metallocene-naphthalimide derivatives: The effect of geometry, DFT methodology, and transition metals on absorption spectra, *Molecules*, 2023, **28**, 3565.
16 R. S. Nobuyasu, J. S. Ward, J. Gibson, B. A. Laidlaw, Z. Ren, P. Data, A. S. Batsanov, T. J. Penfold, M. R. Bryce and F. B. Dias, The influence of molecular geometry on the efficiency of thermally activated delayed fluorescence, *J. Mater. Chem. C*, 2019, **7**, 6672–6684.
17 T. S. Almutairi, Phase transitions and spectral shifts: a quantum mechanical exploration of vibrational frequency in magnesium ferrite, *RSC Adv.*, 2024, **14**, 2727–2740.
18 I. Brandão, H. C. Georg, M. A. Castro and T. L. Fonseca, Calculation of the geometry, absorption spectrum, and first hyperpolarizability of 4,5-dicyanoimidazole derivatives in solution. A multiscale ASEC–FEG study, *J. Chem. Phys.*, 2024, **161**, 034503.
19 D. Tzeli, T. Mercouris, G. Theodorakopoulos and I. D. Petsalakis, Time-evolution study of photoinduced charge-transfer in tertiary amine-fluorophore systems, *Comp. Theor. Chem.*, 2017, **1115**, 197–207.
20 V. Stalin Elanchezhian, E. Kasirajan, P. Muthirulan, P. Muthukrishnan and M. Kandaswamy, Ferrocene-based chemosensor creates molecular logic circuit for selective detection of Hg^{2+} and Cu^{2+}, *J. Mol. Struct.*, 2024, **1313**, 138687.
21 F. J. de Lera-Garrido, V. Vázquez-Villar, M. P. Fernández-Liencres, A. Sánchez-Ruiz, A. Navarro, J. Tolosa and J. C. García-Martínez, Design of large Stokes shift

fluorescent ortho-bis-styrylbenzenes. Optical characterization and fluoride sensing in logical gates, *Dyes Pigm.*, 2024, **225**, 112035.

22 A. V. Ashwathi, N. S. P. Bhuvanesh and S. M. Basheer, Functionalised anthracene chemosensors: kinetics and molecular logic gate operations, *Res. Chem. Intermed.*, 2024, **51**, 1113–1132.

23 C. Adamo and V. Barone, Toward reliable density functional methods without adjustable parameters: The PBE0 model, *J. Chem. Phys.*, 1999, **110**, 6158–6170.

24 J. P. Perdew, K. Burke and M. Ernzerhof, Generalized Gradient Approximation Made Simple, *Phys. Rev. Lett.*, 1996, **77**, 3865–3868.

25 L. A. Curtiss, M. P. McGrath, J.-P. Blaudeau, N. E. Davis, R. C. Binning Jr. and L. Radom, Extension of Gaussian-2 theory to molecules containing third-row atoms Ga–Kr, *J. Chem. Phys.*, 1995, **103**, 6104.

26 S. Miertuš, E. Scrocco and J. Tomasi, Electrostatic interaction of a solute with a continuum. A direct utilizaion of AB initio molecular potentials for the prevision of solvent effects, *Chem. Phys.*, 1981, **55**, 117–129.

27 J. Tomasi, B. Mennucci and R. Cammi, Quantum Mechanical Continuum Solvation Models, *Chem. Rev.*, 2005, **105**, 2999–3094.

28 F. Weigend and R. Ahlrichs, Balanced basis sets of split valence, triple zeta valence and quadruple zeta valence quality for H to Rn: Design and assessment of accuracy, *Phys. Chem. Chem. Phys.*, 2005, **7**, 3297–3305.

29 G. D. Jacquemin, A. Planchat, C. Adamo and B. Mennucci, TD-DFT Assessment of Functionals for Optical 0–0 Transitions in Solvated Dyes, *J. Chem. Theory Comput.*, 2012, **8**, 2359–2372.

30 C. A. Guido, E. Brémond, C. Adamo and P. Cortona, Communication: One third: A new recipe for the PBE0 paradigm, *J. Chem. Phys.*, 2013, **138**, 021104.

31 P. Morgante and R. Peverati, Comparison of the Performance of Density Functional Methods for the Description of Spin States and Binding Energies of Porphyrins, *Molecules*, 2023, **28**, 3487.

32 J.-D. Chai and M. Head-Gordon, Long-range corrected hybrid density functionals with damped atom-atom dispersion corrections, *Phys. Chem. Chem. Phys.*, 2008, **10**, 6615–6620.

33 J. Tao, J. P. Perdew, V. N. Staroverov and G. E. Scuseria, Climbing the Density Functional Ladder: Nonempirical Meta-Generalized Gradient Approximation Designed for Molecules and Solids, *Phys. Rev. Lett.*, 2003, **91**, 146401.

34 S. Grimme, J. Antony, S. Ehrlich and H. Krieg, A consistent and accurate ab initio parameterization of density functional dispersion correction (DFT-D) for the 94 elements H-Pu, *J. Chem. Phys.*, 2010, **132**, 154104.

35 (*a*) M. Caricato, B. Mennucci, J. Tomasi, F. Ingrosso, R. Cammi, S. Corni and G. Scalmani, Formation and relaxation of excited states in solution: A new time dependent polarizable continuum model based on time dependent density functional theory, *J. Chem. Phys.*, 2006, **124**, 124520; (*b*) C. A. Guido and S. Caprasecca, How to Perform Corrected Linear Response Calculations in G09, Dipartimento di Chimica e Chimica Industriale, Universita di Pisa, Pisa, 2016, DOI: 10.13140/RG.2.1.1903.7845.

36 M. J. Frisch, G. W. Trucks, H. B. Schlegel, G. E. Scuseria, M. A. Robb, J. R. Cheeseman, G. Scalmani, V. Barone, B. Mennucci, G. A. Petersson *et al.*, *Gaussian 16, Revision C.01*; Gaussian, Inc., Wallingford CT, 2022.

37 I. Skarmoutsos, D. Tzeli and I. D. Petsalakis, Hydration structure and dynamics, ultraviolet-visible and fluorescence spectra of caffeine in ambient liquid water. A combined classical molecular dynamics and quantum chemical study, *J. Mol. Liquids*, 2023, **391**, 123220.